AIP | The Journal of Chemical Physics

Vibrational state-selective autodetachment photoelectron spectroscopy from dipole-bound states of cold 2-hydroxyphenoxide: o − HO(C6H4)O−

Dao-Ling Huang, Hong-Tao Liu, Chuan-Gang Ning, and Lai-Sheng Wang

Citation: The Journal of Chemical Physics **142**, 124309 (2015); doi: 10.1063/1.4916122
View online: http://dx.doi.org/10.1063/1.4916122
View Table of Contents: http://scitation.aip.org/content/aip/journal/jcp/142/12?ver=pdfcov
Published by the AIP Publishing

Vibrational state-selective autodetachment photoelectron spectroscopy from dipole-bound states of cold 2-hydroxyphenoxide: *o*-HO(C_6H_4)O^-

Dao-Ling Huang,[1] Hong-Tao Liu,[1,2] Chuan-Gang Ning,[3] and Lai-Sheng Wang[1,a)]
[1]*Department of Chemistry, Brown University, Providence, Rhode Island 02912, USA*
[2]*Shanghai Institute of Applied Physics, Chinese Academy of Sciences, Shanghai 201800, China*
[3]*Department of Physics, State Key Laboratory of Low-Dimensional Quantum Physics, Tsinghua University, Beijing 100084, China*

(Received 12 February 2015; accepted 12 March 2015; published online 26 March 2015)

We report a photodetachment and high-resolution photoelectron imaging study of cold 2-hydroxyphenoxide anion, *o*-HO(C_6H_4)O^-, cooled in a cryogenic ion trap. Photodetachment spectroscopy revealed a dipole-bound state (DBS) of the anion, 25 ± 5 cm^{-1}, below the detachment threshold of 18 784 ± 5 cm^{-1} (2.3289 ± 0.0006 eV), i.e., the electron affinity of the 2-hydroxyphenoxy radical *o*-HO(C_6H_4)O˙. Twenty-two vibrational levels of the DBS are observed as resonances in the photodetachment spectrum. By tuning the detachment laser to these DBS vibrational levels, we obtain 22 high-resolution resonant photoelectron spectra, which are highly non-Franck-Condon due to mode-selective autodetachment and the $\Delta v = -1$ propensity rule. Numerous Franck-Condon inactive vibrational modes are observed in the resonant photoelectron spectra, significantly expanding the vibrational information that is available in traditional high-resolution photoelectron spectroscopy. A total of 15 fundamental vibrational frequencies are obtained for the *o*-HO(C_6H_4)O˙ radical from both the photodetachment spectrum and the resonant photoelectron spectra, including six symmetry-forbidden out-of-plane modes as a result of resonant enhancement. © *2015 AIP Publishing LLC.* [http://dx.doi.org/10.1063/1.4916122]

I. INTRODUCTION

Vibrational autodetachment spectroscopy can be a powerful technique to obtain infrared spectra of anions and probe the non-adiabatic intramolecular dynamics between the vibrating neutral core and the outgoing electron.[1–6] However, it cannot be generally applicable because the probed vibrational levels of the anion must be above the electron detachment threshold for autodetachment to occur. Only a limited set of weakly bound anions have been reported with low enough electron binding energies to realize vibrational autodetachment within the ground electronic state.[1–8] Valence excited electronic states of anions are also not usually accessible.[9–16] However, the existence of dipole-bound states (DBSs) near the detachment threshold of anions significantly expands the scope of vibrational autodetachment spectroscopy. A molecule with a large enough dipole moment (>2.5 D) can weakly attract an electron and form a DBS of the corresponding anion in the dipolar field, which was first predicted theoretically[17–20] and has been observed experimentally.[21–27] In dipole-bound anions, the extra electron resides in a highly diffuse orbital outside the neutral core, analogous to Rydberg states in neutral molecules. While anions cannot have Rydberg states, excited DBSs near the detachment threshold are possible if the corresponding neutrals possess a sufficiently large dipole moment. Such excited DBSs were first observed in photodetachment cross sections of enolate anions by Brauman and co-workers.[28–31] Lineberger, Brauman, and co-workers subsequently observed rotational autodetachment via the excited DBS and obtained high-resolution spectroscopy for dipole-bound anions.[32–39] However, due to spectral congestions at room temperature, especially for large and complex anions, such high-resolution detachment spectroscopy has applied only to a limited number of anions. In particular, high-resolution vibrational state-selective autodetachment photoelectron spectroscopy (PES) from a DBS has not been reported until recently.[40]

In 2013, we observed the first mode-specific vibrational autodetachment photoelectron (PE) spectra from the DBS of cold phenoxide anions.[40] In this study, the phenoxide anions were cooled cryogenically in an ion trap to completely eliminate vibrational hot bands and minimize rotational broadening.[41–43] In addition to obtaining high-resolution PE spectra, a DBS was observed 97 cm^{-1} below the detachment threshold of phenoxide. A series of highly non-Franck Condon PE spectra were observed due to excitation of specific vibrational levels of the DBS and the subsequent mode-specific vibrational autodetachment. The $\Delta v = -1$ vibrational propensity rule for autodetachment, which was initially developed for autoionization from Rydberg states[44] and extended to vibration-induced electron detachment of anions,[45,46] was directly observed. In addition, the vibrational frequencies of the DBS of the anion were measured to be the same as the neutral within the experimental uncertainty, confirming that the outmost electron in the DBS of the anion indeed has little effect on the neutral core. This work also suggested that high-resolution vibrational autodetachment from DBS can be used to obtain vibrational spectroscopy of the corresponding neutral radicals, as demonstrated shortly for the dehydrogenated uracil

a)Email: Lai-Sheng_Wang@brown.edu

radical.[47] In the latter study, a total of 46 vibrational autodetachment resonances were observed in the photodetachment spectrum, allowing 21 fundamental vibrational frequencies to be obtained for the dehydrogenated uracil radical.

The 2-hydroxyphenoxy radical, *o*-HO(C_6H_4)O˙, is an important derivative of the phenoxy radical involved in a wide range of biological and environmental processes.[48–50] In particular, *o*-HO(C_6H_4)O˙ has been identified as a persistent environmental free radical formed by decomposition of pyrocatechol in tobacco smoke, which has adverse effects on human health.[51–53] There have been a number of theoretical studies about the conformations of *o*-HO(C_6H_4)O˙,[54–57] however, experimental structural information about *o*-HO(C_6H_4)O˙ has been limited. The *o*-HO(C_6H_4)O˙ radical was observed in a low-temperature matrix-isolation IR spectroscopy study.[56] A previous PES study gave an electron affinity (EA) of 2.315 ± 0.010 eV for *o*-HO(C_6H_4)O˙, along with two vibrational frequencies, 605 (40) cm^{-1} and 1575 (40) cm^{-1}, and theoretical calculations.[58] As expected, the structures of *o*-HO(C_6H_4)O$^-$ and *o*-HO(C_6H_4)O˙ involve H-bonding between the hydroxyl group and the neighboring oxygen atom.

Here, we report both photodetachment spectroscopy and high-resolution PES for *o*-HO(C_6H_4)O$^-$, cooled in a low-temperature ion trap at 4.4 K. A DBS is found for *o*-HO(C_6H_4)O$^-$ and 22 vibrational levels of the DBS are observed in the photodetachment spectrum. Mode-specific vibrational autodetachment is observed in resonant PES via the vibrational levels of the DBS, resulting in highly non-Franck-Condon PE spectra and providing critical information for the assignments of the vibrational resonances in the photodetachment spectrum. The EA of *o*-HO(C_6H_4)O˙ is measured accurately to be 18 784 ± 5 cm^{-1} (2.3289 ± 0.0006 eV). The ground vibrational level of the DBS is measured using resonant two-photon detachment, resulting in a binding energy of 25 ± 5 cm^{-1} for the DBS relative to the detachment threshold. Fifteen fundamental vibrational frequencies are obtained for the *o*-HO(C_6H_4)O˙ radical from both the photodetachment spectrum and the resonant PE spectra.

II. EXPERIMENTAL METHODS

The experiment was carried out using our high-resolution PE imaging apparatus[59] equipped with an electrospray ionization (ESI) source,[60] a temperature-controlled cryogenic ion trap,[41,42] and a time-of-flight mass spectrometer. The apparatus is an improved version based on our original ESI-PES instrument that consisted of a room-temperature ion trap and a magnetic-bottle PES analyzer.[60–62] The *o*-HO(C_6H_4)O$^-$ anions were produced by electrospray of a 1 mM solution of 2-hydroxyphenol dissolved in a mixed methanol and water solvent (9:1 volume ratio). The anions were directed by two radio-frequency (RF) quadrupole ion guides and one RF-only octopole ion guide into a temperature-controlled cryogenically cooled three-dimensional Paul trap in a more compact linear configuration,[42] compared with our first generation cold ion trap.[41] After being accumulated and cooled via collisions with a He/H_2 buffer gas (4:1 volume ratio) in the ion trap for 0.1 s, the anions were pulsed out into the extraction zone of a time-of-flight mass spectrometer and selected by a mass gate. The desirable anions were focused into the interaction zone of a co-linear velocity-map imaging lens,[59] where anions were photodetached by a linear polarized laser beam. The laser polarization was aligned parallel to the imaging detector. Photoelectrons were accelerated out of the imaging lens and projected onto a set of 75-mm diameter micro-channel plates coupled to a phosphor screen. The photoelectron images were captured by a charge-coupled device camera and sent to a computer for data averaging. The recorded two-dimensional PE images were symmetrized and inverse-Abel transformed to obtain three-dimensional photoelectron distributions. The data reconstruction was carried out by both the pBASEX[63] and BASEX programs,[64] which gave similar results.

The velocity-map imaging apparatus was calibrated with PE images of atomic Au^- at several photon energies. The photodetachment laser is a Nd:YAG pumped tunable dye laser system ($\Delta\lambda \sim 0.0015$ nm, Sirah Cobra-Stretch). The experiments reported in the current work were all done by operating the ion trap at 4.4 K. The PE spectra are all plotted with respect to electron binding energies obtained by subtracting the measured electron kinetic energies (KE) from the respective detachment photon energies. The PE spectral resolution achieved was 3.8 cm^{-1} for 55 cm^{-1} KE electrons and about 1.5% (ΔKE/KE) for KE above 1 eV.

III. RESULTS

A. Non-resonant photoelectron images and spectra

Fig. 1 shows the regular non-resonant PE images and spectra of *o*-HO(C_6H_4)O$^-$ at three photon energies. The 488.32 nm spectrum in Fig. 1(c) is relatively congested,

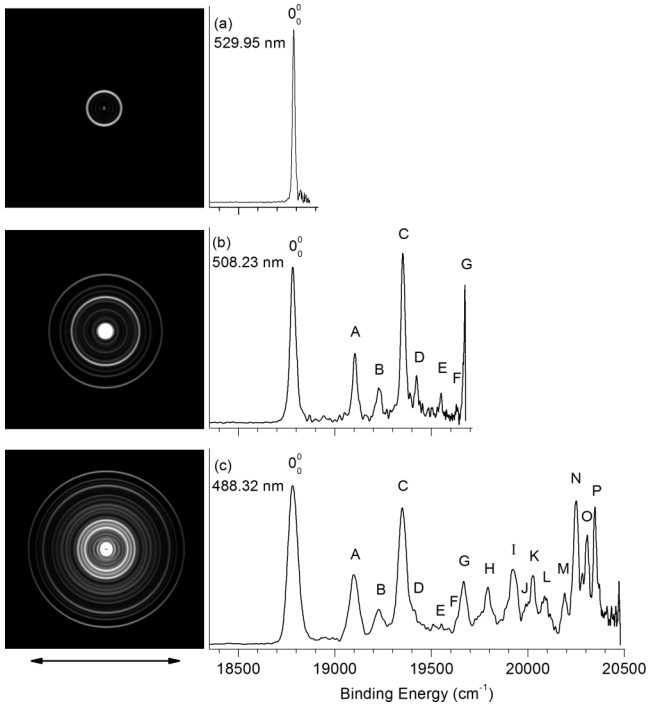

FIG. 1. Non-resonant photoelectron images and spectra of *o*-HO(C_6H_4)O$^-$ at (a) 529.95 nm, (b) 508.23 nm, and (c) 488.32 nm and 4.4 K ion trap temperature. The double arrow below the images indicates the direction of the laser polarization.

TABLE I. Observed BE, shifts from the 0_0^0 transition, and assignments of the resolved vibrational peaks from photoelectron spectra of *o*-HO(C_6H_4)O$^-$. The labels 0_0^0 and *A*–*P* correspond to those observed in the non-resonant spectra in Fig. 1. Peaks *a*–*l* are from resonant spectra in Figs. 3–5.

Peak	BE (cm^{-1})[a]	Shifts (cm^{-1})	Assignment
0_0^0	18 784(5)	0	Neutral ground state
A	19 102(5)	318	23_0^1
B	19 227(5)	443	22_0^1
C	19 350(5)	566	20_0^1
D	19 422(5)	638	23_0^2
E	19 549(8)	765	$23_0^122_0^1$
F	19 631(8)	847	31_0^2
G	19 667(8)	883	$23_0^120_0^1$
H	19 791(8)	1007	$22_0^120_0^1$
I	19 921(10)	1137	20_0^2
J	19 988(8)	1204	$20_0^123_0^2$
K	20 024(8)	1240	$13_0^1/20_0^131_0^132_0^1$
L	20 088(10)	1304	$12_0^1/23_0^231_0^132_0^1$
M	20 190(10)	1406	$22_0^232_0^2$
N	20 249(10)	1465	$9_0^1/23_0^115_0^1$
O	20 306(10)	1522	$8_0^1/23_0^320_0^1$
P	20 347(8)	1563	$23_0^113_0^1$
a	18 950(8)	166	33_0^1
b	19 047(8)	263	32_0^1
c	19 207(5)	423	31_0^1
d	19 616(8)	832	$32_0^120_0^1$
e	19 307(10)	523	30_0^1
f	19 496(15)	712	29_0^1
g	19 460(10)	676	$31_0^132_0^1$
h	19 525(10)	741	$31_0^123_0^1$
i	19 769(10)	985	$31_0^120_0^1$
j	19 927(8)	1143	15_0^1
k	19 627(10)	843	31_0^2
l	19 780(10)	996	24_0^1

[a]Numbers in parentheses indicate the experimental uncertainties in the last digit. The peaks *A*–*P* are also observed in Figs. 3–5, which give more accurate BEs for some peaks and are used here.

resolving numerous vibrational peaks (labeled by capital letters from *A* to *P*) for the ground electronic state of the neutral *o*-HO(C_6H_4)O$^\cdot$ radical. At 508.23 nm (Fig. 1(b)), peaks *D*, *E*, and *F* are much better resolved. The enhancement of peak *G* in Fig. 1(b) is due to the near threshold effect.[65] The 529.95 nm photon energy is slightly above the detachment threshold and Fig. 1(a) displays the best resolved data for the 0_0^0 transition. The peak width is much larger than the instrumental resolution due to rotational broadening.[40,47] This peak defines a very accurate EA for *o*-HO(C_6H_4)O$^\cdot$ as 18 784 ± 5 cm^{-1} (2.3289 ± 0.0006 eV), measured from the top of the 0_0^0 peak in Fig. 1(a). The 488.32 nm spectrum shows that peak *C* is the strongest vibrational peak, corresponding to the 20_0^1 transition (*vide infra*), suggesting that the ν_{20} mode is the most Franck-Condon-active vibrational mode upon electron detachment. Peak *C* is slightly enhanced in Fig. 1(b), probably also due to the near threshold effect. The PE images in Fig. 1 all show that the photoelectron angular distribution (PAD) has *s* + *d* characters, indicating that the highest occupied molecular orbital (HOMO) of *o*-HO(C_6H_4)O$^-$ is a *p*-type orbital. The near threshold behaviors are consistent with the PAD.

The electron binding energies of all the observed vibrational peaks, their shifts from the 0_0^0 transition, and the assignments are summarized in Table I. The assignments and comparison with theoretical frequencies are given in Table II.

B. Photodetachment spectrum of *o*-HO(C_6H_4)O$^-$: observation of vibrational resonances due to the dipole-bound state

Fig. 2 displays the photodetachment spectrum of *o*-HO(C_6H_4)O$^-$ by measuring the total electron yield as a function of photon energy near the detachment threshold. The scanning photon energy range covers about 1600 cm^{-1}. The scanning step was 0.03 nm and each step was accumulated for 700 laser shots. The overall baseline in Fig. 2 represents the intensity of direct non-resonant photodetachment from the ground state of *o*-HO(C_6H_4)O$^-$ to the neutral ground state, which slowly increases with photon energy. At certain wavelengths, the total electron yields are enhanced dramatically, as indicated by the peaks labeled from 1 to 22. These peaks

TABLE II. Calculated vibrational modes and frequencies for *o*-HO(C_6H_4)O$^\cdot$ and comparison with the experimental values. Harmonic frequencies are calculated with the B3LYP/6-311 + G(d,p) method and are unscaled.

Mode	Symmetry	Theoretical (cm^{-1})	Experimental (cm^{-1})[a]	Peak[b]
υ_1	A′	3562		
υ_2		3200		
υ_3		3195		
υ_4		3184		
υ_5		3172		
υ_6		1609		
υ_7		1575		
υ_8		1527	**1515(8)**	20
υ_9		1488	**1458(8)**	19
υ_{10}		1438		
υ_{11}		1382		
υ_{12}		1334	**1298(8)**	18
υ_{13}		1261	**1237(8)**	17
υ_{14}		1193		
υ_{15}		1169	**1143(8)**	15
υ_{16}		1130		
υ_{17}		1009		
υ_{18}		884		
υ_{19}		755		
υ_{20}		578	**565(5)**	6
υ_{21}		566	**555(8)**	5
υ_{22}		450	**443(5)**	3
υ_{23}		324	**318(5)**	1
υ_{24}	A″	982	996(10)	
υ_{25}		950		
υ_{26}		852		
υ_{27}		771		
υ_{28}		723		
υ_{29}		709	**700(5)**	15
υ_{30}		505	**520(5)**	4
υ_{31}		454	423(8)	
υ_{32}		270	263(8)	
υ_{33}		166	166(8)	

[a]Numbers in parentheses indicate the experimental uncertainties in the last digit. The values in bold face were obtained from photodetachment spectrum of *o*-HO(C_6H_4)O$^-$ shown in Fig. 2. The values in normal font were measured from resonant PE spectra in Figs. 3–5.

[b]The numbers correspond to the labels in Fig. 2.

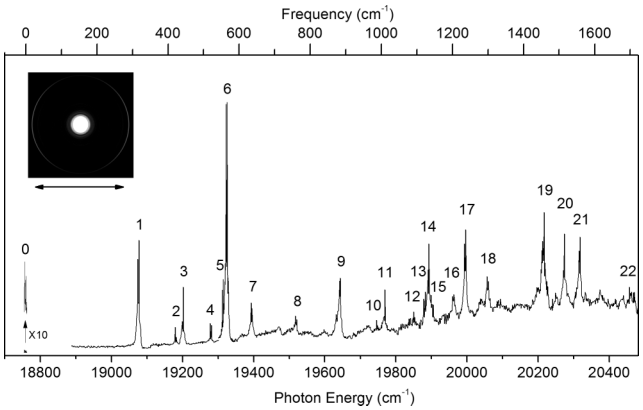

FIG. 2. The photodetachment spectrum of o-HO(C_6H_4)O^- by measuring the total electron yield as a function of photon energy near the detachment threshold. The peaks labeled as 1–22 are due to autodetachment from vibrational levels of a DBS of o-HO(C_6H_4)O^-. The very weak peak labeled as 0 at 18 759 cm^{-1} (expanded by 10 times), is determined to be the dipole-bound ground state. This weak peak is due to single color resonant two-photon (1 + 1) detachment. The inset shows the photoelectron image of the two-photon detachment spectrum, where the outer ring is the two-photon signal. The double arrow below the images indicates the direction of the laser polarization. Note the p-wave character of the two-photon peak, indicating the DBS electron is in an s-like orbital.

provide evidence of the existence of a DBS of o-HO(C_6H_4)O^- and they are due to autodetachment from vibrational levels of the DBS, as shown previously for the phenoxide and deprotonated uracil anions.[40,47] In comparison to the earlier studies by the Brauman and Lineberger groups,[28–39] the critical improvement is the vibrational and rotational cooling afforded by the temperature-controlled cryogenic ion trap. The resonant peaks all have a width of ~5 cm^{-1} with fine features, due to partially resolved rotational profiles. As shown previously,[47] the rotational temperature of our trapped ions was about 35 K at an ion trap temperature of 4.4 K, even though the vibrational temperature could not be evaluated because there were no vibrational hot bands observed.

The very weak peak labeled as 0 at 18 759 cm^{-1}, expanded by 10 times, represents the ground vibrational level of the DBS. This extremely weak peak is due to single color two-photon (1 + 1) detachment, corresponding to the outer ring of the inset PE image. Hence, the binding energy of the DBS was determined to be 25 ± 5 cm^{-1}, relative to the detachment threshold (18 784 cm^{-1}) measured in Fig. 1(a). The top scale of Fig. 2 is relative to the vibrational ground state of the DBS, so that the vibrational energies of the 22 autodetachment resonances can be directly read from the figure. Table III summarizes the photon energies, shifts from the DBS vibrational ground state, and the complete assignments of the observed vibrational resonances. The assignments for peaks 1–22 are all supported by and based on resonant PE spectra to be presented next in Figs. 3–5 and the calculated frequencies in Table II.

The PAD of the two-photon detachment peak in the inset of Fig. 2 shows clearly a p-wave, which is very different from the $s + d$ character of the non-resonant detachment features in Fig. 1. The ground vibrational level of the DBS is bound and long-lived. The PAD in the two-photon detachment should reflect the electronic nature of the DBS, which can be viewed as an s-type orbital, consistent with the observed p-wave PAD.

TABLE III. The observed photon energies, shifts from peak 0, and assignments of the vibrational autodetachment resonances in Fig. 2.

Peak	Photon energy (cm^{-1})[a]	Shift (cm^{-1})	Assignment
0	18 759(5)	0	DB ground state
1	19 077(5)	318	$23_0'^1$
2	19 179(5)	420	$32_0'^1 33_0'^1$
3	19 202(5)	443	$22_0'^1$
4	19 279(5)	520	$30_0'^1/32_0'^2$
5	19 314(8)	555	$21_0'^1$
6	19 324(5)	565	$20_0'^1$
7	19 393(5)	634	$23_0'^2$
8	19 514(5)	755	$23_0'^1 22_0'^1$
9	19 643(5)	884	$20_0'^1 23_0'^1$
10	19 746(5)	987	$20_0'^1 31_0'^1$
11	19 769(5)	1010	$22_0'^1 20_0'^1$
12	19 850(5)	1091	$20_0'^1 30_0'^1$
13	19 881(5)	1122	$20_0'^1 21_0'^1$
14	19 893(5)	1134	$20_0'^2$
15	19 902(8)	1143	$15_0'^1/22_0'^1 29_0'^1$
16	19 963(5)	1204	$23_0'^2 20_0'^1$
17	19 996(8)	1237	$13_0'^1/20_0'^1 31_0'^1 32_0'^1$
18	20 057(8)	1298	$12_0'^1/20_0'^1 23_0'^1 31_0'^1$
19	20 217(8)	1458	$9_0'^1/23_0'^1 15_0'^1$
20	20 274(8)	1515	$8_0'^1/23_0'^3 20_0'^1$
21	20 318(8)	1559	$23_0'^1 13_0'^1/20_0'^1 24_0'^1$
22	20 457(5)	1698	$20_0'^3$

[a]Numbers in parentheses indicate the experimental uncertainties in the last digit.

C. Resonant photoelectron images and spectra

By tuning the detachment laser to the vibrational resonances observed in Fig. 2, we obtained resonantly enhanced PE spectra, as shown in Figs. 3–5. These spectra contain two detachment processes, the regular non-resonant photodetachment represented by the baseline of Fig. 2 and resonantly enhanced vibrational autodetachment signals via the DBS. The resonant enhancement can be glimpsed from the peak height relative to the baseline at each photon energy in Fig. 2. The 22 resonant PE spectra are presented in Figs. 3–5 according to the nature of the vibrational levels of the DBS excited: the spectra in Fig. 3 correspond to the excitation of a single vibrational mode of the DBS; those in Fig. 4 represent excitations to combinational vibrational levels of the DBS involving two modes; those in Fig. 5 correspond to excitations to overlapping vibrational levels of the DBS. Because of the mode selectivity and the $\Delta v = -1$ propensity rule in the autodetachment process,[44] certain vibrational levels are enhanced in each resonant PE spectrum, resulting in completely non-Franck-Condon distributions relative to the non-resonant PE spectra in Fig. 1. Furthermore, Franck-Condon inactive modes are observed in the resonant PE spectra and these transitions are labeled by lower case letters in Figs. 3–5. Their binding energies and assignments are also given in Table I.

In Figs. 3–5, the assigned vibrational transitions in bold face indicate the final vibrational states of autodetachment, that are resonantly enhanced. It should also be pointed out that the binding energies in Table I, for the vibrational peaks observed in Fig. 1, are taken from the more accurate measurements in the resonant spectra, wherever possible.

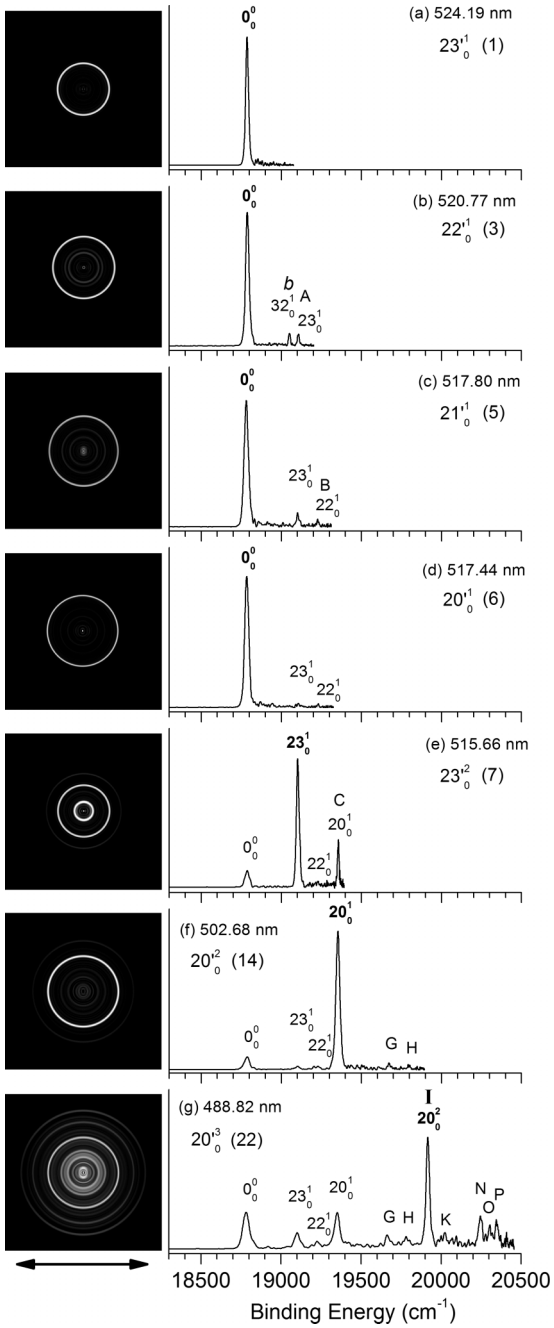

FIG. 3. Resonant photoelectron images and spectra of o-$HO(C_6H_4)O^-$ at seven different detachment wavelengths, corresponding to the resonance peaks in Fig. 2. The peak number (in parentheses) and the vibrational levels of the DBS are given. The double arrow below the images indicates the direction of the laser polarization. The labels in capital letters are the same as in Fig. 1 and those in bold face indicate the autodetachment-enhanced final vibrational states.

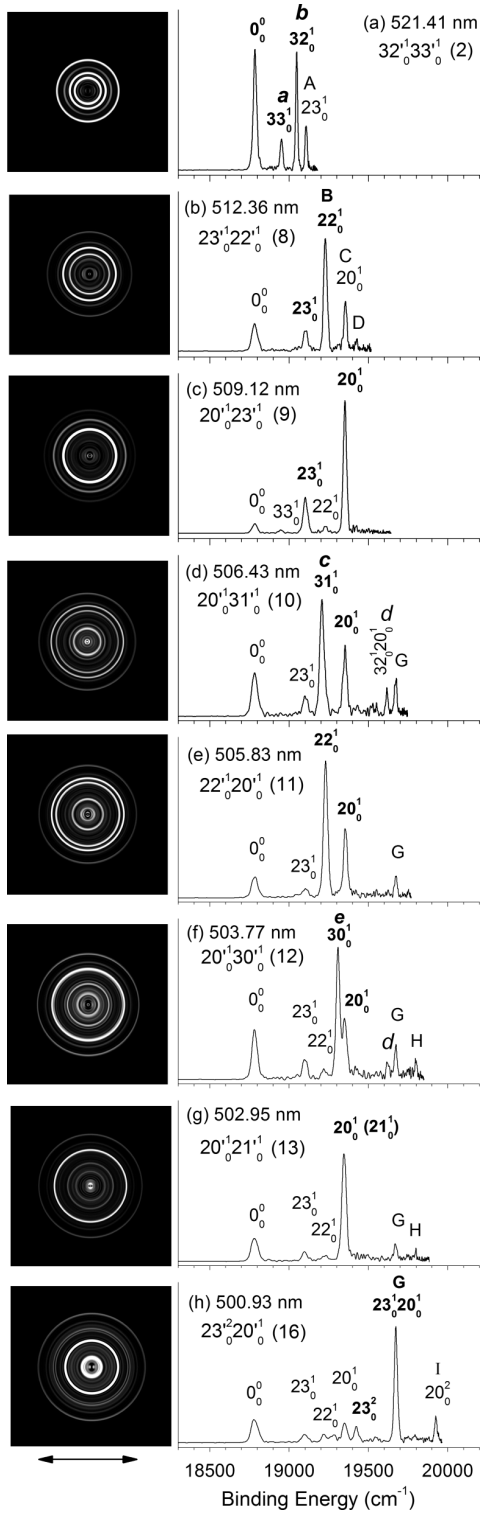

FIG. 4. Resonant photoelectron images and spectra of o-$HO(C_6H_4)O^-$ at eight different detachment wavelengths, corresponding to the resonance peaks in Fig. 2. The peak number (in parentheses) and the vibrational levels of the DBS are given. The double arrow below the images indicates the direction of the laser polarization. The labels in capital letters are the same as in Fig. 1 and those in bold face indicate the autodetachment-enhanced final vibrational states.

IV. DISCUSSION

A. Assignment of the non-resonant photoelectron spectra

While the previous low resolution PE spectra revealed only two vibrational modes tentatively for the ground state detachment band,[58] the high-resolution PE spectra in Fig. 1 suggest that many vibrational modes are active upon photodetachment from o-$HO(C_6H_4)O^-$. To assist the assignment of the observed vibrational structure, we carried out density functional theory (DFT) calculations at the B3LYP/6-311++ (d, p) level for the vibrational frequencies of the o-$HO(C_6H_4)O^{\cdot}$ radical, as given in Table II. Since non-resonant PE spectra

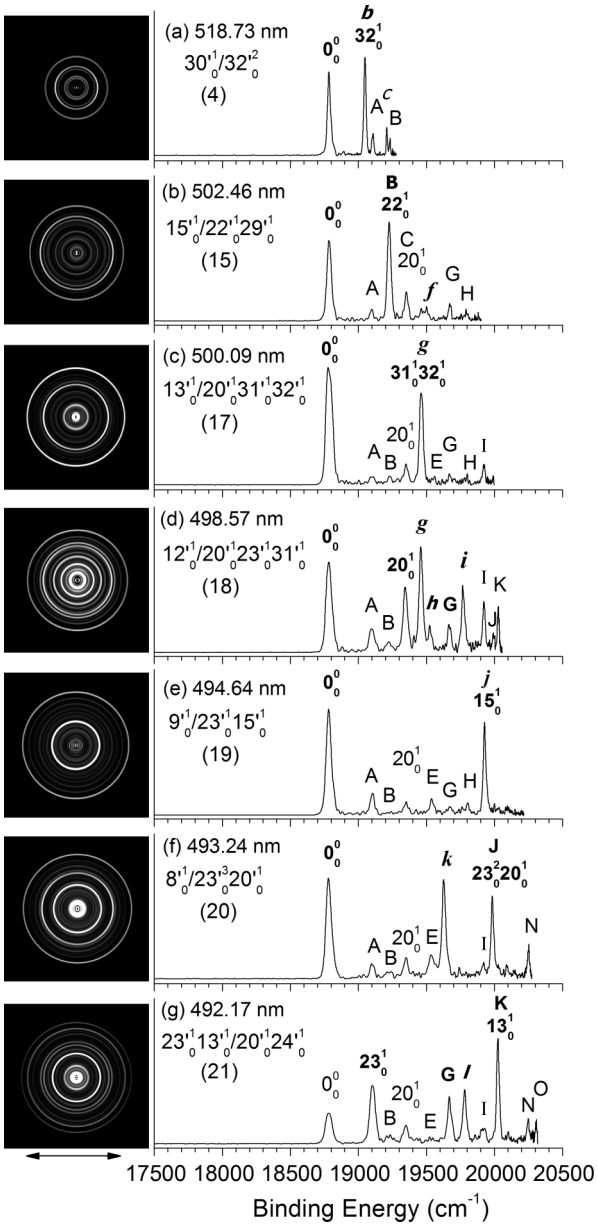

FIG. 5. Resonant photoelectron images and spectra of o-HO(C_6H_4)O^- at seven different detachment wavelengths, corresponding to the resonance peaks in Fig. 2. The peak number (in parentheses) and the vibrational levels of the DBS are given. The double arrow below the images indicates the direction of the laser polarization. The labels in capital letters are the same as in Fig. 1 and those in bold face indicate the autodetachment-enhanced final vibrational states.

represent Franck-Condon-active vibrational modes for the ground state detachment transition, only symmetry-allowed modes are supposed to be observed. The o-HO(C_6H_4)O$^\cdot$ radical has C_s symmetry, hence, all in-plane vibration modes (a′) or even quanta of out-of-plane modes (a″) are symmetry-allowed. By comparing the theoretical frequencies and the experimental shifts from the 0_0^0 peak in Table I for peaks *A*–*P*, we can readily assign peaks *A*, *B*, *C*, *K*, *L*, *N*, and *O* to modes υ_{23}, υ_{22}, υ_{20}, υ_{13}, υ_{12}, υ_9, and υ_8, respectively. Peaks *D* and *I* are due to the overtones of modes υ_{23} and υ_{20}, respectively. Peak *F* could be due to the overtone of the out-of-plane mode υ_{31}. Peaks *E*, *G*, *H*, *J*, *M*, and *P* are all due to combinational vibrational levels involving two vibrational modes, as shown in Table I. Finally, two possible assignments are made for several high binding energy peaks, *F*, *K*, *L*, *N*, and *O*. As will be shown below, all these assignments are confirmed by the photodetachment spectrum and the resonant PE spectra via the observation of mode-selective vibrational autodetachment.

B. Nature and assignment of the photodetachment spectrum

All the 22 resonant peaks in the photodetachment spectrum of Fig. 2 are rotationally broadened and they exhibit asymmetric or Fano line shapes in the baseline due to interference effects between the direct detachment and resonant autodetachment channels.[66,67] As we showed previously,[40,47] the vibrational frequencies of the DBS of the anions are the same as the corresponding neutral radical within our experimental uncertainty. Therefore, the vibrational frequencies observed for the DBS of o-HO(C_6H_4)O^- in Fig. 2 should be the same as those of the o-HO(C_6H_4)O$^\cdot$ radical observed in the PE spectra of Fig. 1. Since the photodetachment spectrum of o-HO(C_6H_4)O^- is mainly limited by rotational broadening (~5 cm^{-1} peak width), the measured frequencies from Fig. 2 should be generally more accurate than those obtained from the PE spectra. Comparing Tables I and II, we can see that almost all the vibrational peaks observed in the PE spectra in Fig. 1 can be found in the photodetachment spectrum. The experimental vibrational frequencies given in Table II represent the most accurate measurements in the current work. More vibrational levels were observed in the photodetachment spectrum because of the higher sensitivity as a result of the resonant excitation to the DBS. Combining this spectrum and the resonant PE spectra, we were able to obtain a total of 15 fundamental vibrational frequencies for the o-HO(C_6H_4)O$^\cdot$ radical, including six out of plane modes, as shown in Table II.

The relative intensities of the vibrational resonances in Fig. 2 exhibit large variations with peak 6 being the strongest. Peak 6 is due to excitation to the $20'_0{}^1$ level of the DBS, which corresponds to the most intense peak *C* in the PE spectra of Fig. 1. Because the autodetachment rate is fast from the DBS, the relative intensities of all the vibrational resonances should be proportional to the Franck-Condon factors between the ground vibrational state of o-HO(C_6H_4)O^- and the vibrational levels of the DBS. A careful comparison of Fig. 2 with the non-resonant PE spectrum of Fig. 1(c) reveals similar intensity distributions for all the peaks of the same vibrational modes. For example, the relative intensities of the 14 major resonant peaks, 1, 3, 6, 7, 8, 9, 11, 14, 16, 17, 18, 19, 20, and 21 in Fig. 2 resemble the overall Franck-Condon envelope of peaks *A*, *B*, *C*, *D*, *E*, *G*, *H*, *I*, *J*,*K*, *L*, *N*, *O*, and *P* in Fig. 1(c), respectively. In other words, the Franck-Condon factors between the ground vibrational state and the vibrational levels of the DBS of o-HO(C_6H_4)O^- and those between the ground vibrational state of o-HO(C_6H_4)O^- and the corresponding vibrational levels of the neutral ground electronic state of o-HO(C_6H_4)O$^\cdot$ are similar. This observation further confirms that the extra electron in the DBS is weakly bonded and has little effect on the neutral core, just like in a Rydberg state for a neutral molecule.

In addition to the Franck-Condon active modes, several Franck-Condon forbidden transitions were also observed in the photodetachment spectrum of Fig. 2, such as $30'_0{}^1$ (Peak 4), $20'_0{}^1 31'_0{}^1$ (Peak 10), $20'_0{}^1 30'_0{}^1$ (Peak 12), and $22'_0{}^1 29'_0{}^1$ (Peak 15). Even though the relative intensities of these transitions were low, they were clearly observable and yielded several vibrational frequencies for the bending modes (Table II) in the resonant PE spectra to be discussed below. The observation of such transitions might be partly due to significant resonant enhancement in the optical transitions from the anion ground state to those of the DBS. They might also be due to strong vibronic coupling in the DBS of *o*-HO(C_6H_4)O^-. It should be pointed out that such symmetry-forbidden transitions have also been observed in high resolution PES of anions,[68] including those of cold phenoxide and C_{60}^-.[40,43] The elimination of vibrational hot bands in the anions has made it much easier to spot such weak transitions in both PES and photodetachment spectroscopy.

C. General comments for vibrational autodetachment from a dipole-bound state

Because the molecular core of the DBS is similar to the neutral state, the harmonic oscillator vibrational selection rule of $\Delta v = -1$ is obeyed in the autodetachment from the DBS to the neutral final state, just like vibrational autoionization from Rydberg states.[40,44,45] In other words, the nth overtone of a given mode (v_x') of the DBS can only autodetach to the $(n-1)$ vibrational level of the corresponding mode (v_x) in the neutral final state. Essentially, one vibrational quantum of the neutral core is coupled to the DBS electron to cause electron emission. The kinetic energy of the outgoing electron corresponds to the vibrational quantum minus the binding energy of the DBS (see Fig. 6). The $\Delta v = -1$ propensity rule can be violated if there are significant anharmonic effects, allowing $\Delta v = -2, -3, \ldots$ autodetachment to be observed.[44] Since the binding energy of the DBS of *o*-HO(C_6H_4)O^- is very small (i.e., 25 ± 5 cm^{-1}), a single-quantum excitation of any vibrational mode in the DBS can induce autodetachment. In cases of combinational modes ($v_x'v_y'$), there can be two possible autodetachment channels involving either modes, while each obeying the $\Delta v = -1$ propensity rule. Hence, a specific vibrational level of a given mode (v_x) would be enhanced in the resonant PE spectrum, if the corresponding mode (v_x') is involved in the DBS vibrational excitation, giving rise to the non-Franck-Condon profile. Thus, the resonant PE spectra can be quite readily understood, and are essential to assign the vibrational resonances in the photodetachment spectrum in Fig. 2. The only complications occur when there are overlapping vibrational levels in a given DBS resonance, which occurs more commonly in the higher energy regime due to high densities of vibrational levels. In such cases, multiple autodetachment channels are possible, but still the resulting resonant PE spectra can be readily assigned.

To help interpret the resonant PE spectra and understand the autodetachment processes, we present an energy level diagram in Fig. 6, showing the direct detachment transition to the vibrational levels of neutral *o*-HO(C_6H_4)O$^\cdot$ (middle) and the 22 vibrational levels of the DBS of *o*-HO(C_6H_4)O^- (left and right) observed in Fig. 2. The EA of *o*-HO(C_6H_4)O$^\cdot$ and the binding energy of the DBS are also given in Fig. 6. Autodetachment from the vibrational levels of the DBS to the neutral final states is indicated by the arrows. Multiple autodetachment channels from the same DBS level are

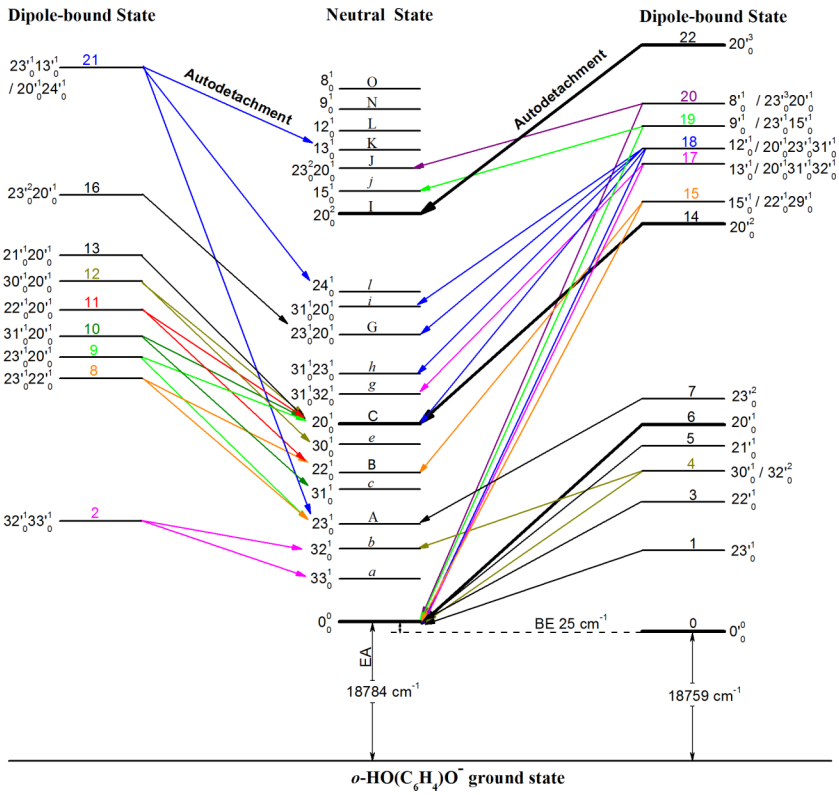

FIG. 6. Schematic energy level diagram for direct detachment from the ground state of *o*-HO(C_6H_4)O^- to the vibrational levels of the ground electronic state of neutral *o*-HO(C_6H_4)O$^\cdot$ (middle) (the labels *A*–*O* are the same as Fig. 1 and *a*–*j* are the same as in Figs. 3–5). The DBS and its 22 vibrational levels observed in Fig. 2 are shown on the left and right side. The EA and BE of the DBS are indicated. Autodetachment channels from the DBS vibrational levels to the neutral final states are indicated by the arrows. On the right side, the vibrational levels of a single mode are indicated and the overlapping vibrational levels in a number of cases are also shown. On the left, combinational vibrational levels of the DBS involving two modes are shown. Autodetachment channels from the same vibrational levels are shown in the same color. See Table III for the detailed assignment of the DBS vibrational levels.

represented by the same color. On the right of Fig. 6, we present all the DBS vibrational resonances involving single vibrational mode, except peaks 4, 15, 17, 18, 19, and 20, which contain overlapping vibrational levels. On the left of Fig. 6, we show the DBS vibrational resonances of combinational vibrational levels involving two modes, except peak 21, which contains an overlapping vibrational level.

Note that the neutral vibrational levels labeled with the capital letters (*A*–*O*) are the same as in Fig. 1 and Table I. Neutral vibrational levels labeled with the lower case letters (*a*–*j*) are observed in the resonant PE spectra due to autodetachment. The vibrational levels for the most active mode (v_{20} and v_{20}') are drawn with thicker lines. The detailed assignments for all the DBS vibrational resonances are given in Table III.

D. Resonant PES involving autodetachment from vibrational levels of a single vibrational mode of the DBS

The 0_0^0 transition in Figs. 3(a)–3(d) is significantly enhanced, indicating autodetachment from a fundamental excitation ($\nu'_0{}^1$) of a single vibrational mode of the DBS of *o*-$HO(C_6H_4)O^-$ in each case. The PADs for the 0_0^0 peak in the PE images of Figs. 3(a)–3(d) are all isotropic, different from the $s + d$ character shown in the non-resonant PE spectra in Fig. 1, consistent with the fact that the electron signals are predominantly due to autodetachment from the DBS of *o*-$HO(C_6H_4)O^-$. As shown in Table III and also labeled in Fig. 3, the detachment energies used for Figs. 3(a)–3(d) correspond to resonant excitations to the $23'_0{}^1$, $22'_0{}^1$, $21'_0{}^1$, and $20'_0{}^1$ vibrational levels of the DBS, respectively. Autodetachment from these levels to the neutral 0_0^0 level is indicated in Fig. 6. The weak PES peaks, 23_0^1 and 22_0^1 in Figs. 3(b)–3(d), are Franck-Condon active transitions and they represent non-resonant detachment transitions. The intensity ratios of the 0_0^0 peak relative to the 23_0^1 peak in Figs. 3(b)–3(d) should correspond roughly to the ratios of the resonant peaks 3, 5, and 6 relative to the non-resonant baseline signals in Fig. 2. For example, Fig. 3(d) shows that peak 23_0^1 due to non-resonant detachment is almost negligible relative to the 0_0^0 peak, because peak 6 in Fig. 2 is the strongest transition. However, the weak 32_0^1 peak in Fig. 3(b) is a Franck-Condon forbidden transition, which was not observed in Fig. 1. Although not explicitly discussed, such non-Franck-Condon transitions involving low frequency modes have been observed in our previous phenoxide and deprotonated uracil studies.[40,47] The mechanisms of such transitions in the resonant PE spectra are not completely understood, but could be due to an intramolecular electron re-scattering effect that has been invoked to interpret the observation of forbidden rotational transitions in resonant two-photon PES and autodetachment.[69,70]

Figs. 3(e) and 3(f) show that the 23_0^1 and 20_0^1 neutral vibrational levels are enhanced, suggesting autodetachment from the $23'_0{}^2$ and $20'_0{}^2$ overtones of the DBSs (peaks 7 and 14 in Fig. 2), respectively, as shown in Table III and Fig. 6. The enhancement of the 20_0^1 peak in Fig. 3(e) is likely due to the near threshold effect. Similarly, the 20_0^2 neutral vibrational level is enhanced in Fig. 3(g), corresponding to the excitation of the $20'_0{}^3$ vibrational level of the DBS. The PAD of the 20_0^2 peak in the PE image is again isotropic in Fig. 3(g), whereas all other PES features are very similar to those in Fig. 1(c) and their PADs all exhibit $s + d$ characters, indicating they are all from direct non-resonant photodetachment.

There are more resonances corresponding to fundamental excitations of a single vibrational mode of the DBS, but these resonances also overlap with other vibrational levels, yielding very complicated resonant PE spectra when the detachment lasers were tuned to these resonances, as shown in Fig. 5. The easiest way to identify such excitations is to compare the intensity of the 0_0^0 transition with a direct detachment peak of higher binding energies in the resonant PE spectra to look for non-Franck-Condon distributions. For example, the 0_0^0 peak is significantly enhanced relative to the 20_0^1 peak in Figs. 5(b), 5(c), 5(e), and 5(f), suggesting the excitations of the $15'_0{}^1$, $13'_0{}^1$, $9'_0{}^1$, and $8'_0{}^1$ levels of the DBS, respectively. The 0_0^0 peak is enhanced relative to peaks *A* and *B* in Figs. 5(a) and 5(d), indicating excitations of the $30'_0{}^1$ and $12'_0{}^1$ vibrational levels of the DBS, respectively, as shown in Table III and Fig. 6.

E. Autodetachment from combinational vibrational levels of the DBS

Autodetachment from combinational vibrational levels of the DBS can be quite complicated because different autodetachment channels are possible. Fig. 4 shows the resonant PE spectra when the detachment laser was tuned to excite combinational vibrational levels of the DBS involving two modes. Thus, two autodetachment channels should be observed in each spectrum. Indeed, Fig. 4 shows that in each case, two vibrational peaks are enhanced (labeled in bold face) relative to the nonresonant PE spectra in Fig. 1. Fig. 4(g) involves the resonant excitation to the $20'_0{}^121'_0{}^1$ level of the DBS (peak 13). Because the frequencies of the ν_{20} and ν_{21} modes are close to each other (within 10 cm^{-1}, Table II), the 20_0^1 and 21_0^1 peaks are not resolved in Fig. 4(g). The peak width is consistent with the overlap of the two detachment channels. In each case in Fig. 4, there seems also to be a more favorable final state with a stronger relative intensity. It should be pointed out that both the 32_0^1 and 33_0^1 final neutral vibrational states in Fig. 4(a) are non-Franck-Condon transitions, which were not observed in Fig. 1. However, the corresponding resonant excitation to the $32'_0{}^133'_0{}^1$ level of the DBS was symmetry-allowed, albeit it was quite weak (peak 2 in Fig. 2). The autodetachment from this level, shown in the resonant PE spectrum in Fig. 4(a), allowed us to measure the fundamental vibrational frequencies of the two softest modes of $HO(C_6H_4)O^{\cdot}$ simultaneously (Table II). These low frequencies for the two bending modes would have been quite difficult to measure experimentally otherwise.

The PADs in the PE images in Fig. 4 can also be used to distinguish autodetachment-enhanced vibrational peaks from direct non-resonant PES features. The autodetachment enhanced peaks all show isotropic PADs, while the non-resonant PES peaks display $s + d$ characters. For example, the PE images corresponding to the relatively weak peaks,

such as 0_0^0, 23_0^1, 22_0^1, 20_0^1, and 20_0^2 in Fig. 4(h) are all $s + d$ wave-like, while those corresponding to 23_0^2 and $23_0^120_0^1$ are isotropic.

Excitations to overlapping vibrational levels of the DBS of o-$HO(C_6H_4)O^-$ can result in even more complicated resonant PE spectra, as shown in Fig. 5. Apart from the enhanced 0_0^0 peak, peak 32_0^1 in Fig. 5(a), peaks 22_0^1 and f in Fig. 5(b), peak g in Fig. 5(c), peaks 20_0^1, g, h, G, and i in Fig. 5(d), peak j in Fig. 5(e), and peak k and $23_0^220_0^1$ in Fig. 5(f) are either non-Franck-Condon and not observed in Fig. 1(c) or much stronger than those in Fig. 1(c). The resonant peak 21 of the DBS gives rise to the resonant PE spectrum of Fig. 5(g), which involves the overlap of two combinational vibrational levels. According to the $\Delta v = -1$ vibrational propensity rule, the assignments of the vibrational levels of the DBS that produced the resonant PE spectra as a result of autodetachment are straightforward, as shown in Fig. 6.

The only three peaks that cannot be readily explained are peak g in Fig. 5(d), peak k in Fig. 5(f), and peak G in Fig. 5(g). The assignment of the overlapping $12'_0{}^1$ and $20'_0{}^123'_0{}^121'_0{}^1$ DBS levels in Fig. 5(d) can explain all the enhanced peaks such as 0_0^0, 20_0^1, h, G, and i very well, except peak g with a $31_0^132_0^1$ final state. This peak might be due to the autodetachment from $31'_0{}^132'_0{}^123'_0{}^2$, which is very close to the energy of $12'_0{}^1$ or $20'_0{}^123'_0{}^121'_0{}^1$. This assignment would require the breakdown of the $\Delta v = -1$ propensity rule, because two quanta of $23'_0{}^2$ would be needed to couple with the outgoing electron. Similarly, the assignment of $8'_0{}^1$ and $23'_0{}^320'_0{}^1$ in Fig. 5(f) explains the enhancement of peaks 0_0^0 and $23_0^220_0^1$, but cannot explain peak k (31_0^2). Peak k might be due to the autodetachment from $31'_0{}^332'_0{}^1$, which would also involve the coupling of two vibrational quanta ($31'_0{}^132'_0{}^1$) to the outgoing electron. The coupling of $31'_0{}^132'_0{}^1$ to the outgoing electron can also explain peak G ($23_0^120_0^1$) in Fig. 5(g) due to the autodetachment from the $23'_0{}^120'_0{}^131'_0{}^132'_0{}^1$ combinational level. It is understandable that, at such highly vibrationally excited state of the DBS, both the high density of vibrational states and anharmonicity can give rise to much more complicated autodetachment transitions.

It should also be pointed out that there is a mode-dependence for the autodetachment processes, as shown in Fig. 4. Simons and co-workers have developed theoretical frameworks for computing vibrational autodetachment rates.[45,46] Lineberger and co-workers have observed vibrational dependence of autodetachment rates in H_2CCC^-.[39] The current work provides extensive vibrational and mode-dependent information for the autodetachment rates, which would be interesting for further theoretical investigations.

V. CONCLUSIONS

In conclusion, we report a high-resolution photoelectron imaging and photodetachment study of cold 2-hydroxyphenoxide anions. The electron affinity of o-$HO(C_6H_4)O^{\cdot}$ is accurately measured to be 18 784 ± 5 cm^{-1} (2.3289 ± 0.0006 eV). A dipole-bound state is observed with a binding energy of 25 ± 5 cm^{-1}. Twenty-two vibrational levels of the dipole-bound states, as well as the dipole-bound ground state of o-$HO(C_6H_4)O^-$ are observed. Resonant photoelectron spectra are obtained by tuning the detachment laser to these vibrational levels, resulting in highly non-Franck-Condon photoelectron spectra due to the mode-selective autodetachment. Fifteen fundamental vibrational frequencies are obtained for the o-$HO(C_6H_4)O^{\cdot}$ radical, including six symmetry-forbidden out-of-plane modes as a result of the resonant enhancement.

ACKNOWLEDGMENTS

This work was supported by the National Science Foundation (No. CHE-1263745).

[1]D. M. Neumark, K. R. Lykke, T. Andersen, and W. C. Lineberger, J. Chem. Phys. **83**, 4364 (1985).
[2]C. G. Baily, J. Kim, and M. A. Johnson, J. Phys. Chem. **100**, 16782 (1996).
[3]P. Ayotte, C. G. Baily, J. Kim, and M. A. Johnson, J. Chem. Phys. **108**, 444 (1998).
[4]J. M. Weber, W. H. Robertson, and M. A. Johnson, J. Chem. Phys. **115**, 10718 (2001).
[5]T. Maeyama, I. Yagi, Y. Murota, A. Fujii, and N. Mikami, J. Phys. Chem. A **110**, 13712 (2006).
[6]B. M. Elliot, L. R. McCunn, and M. A. Johnson, Chem. Phys. Lett. **467**, 32 (2008).
[7]H. Schneider, K. M. Vogelhuber, F. Schinle, J. F. Stanton, and J. M. Weber, J. Phys. Chem. A **112**, 7498 (2008).
[8]C. L. Adams, H. Schneider, and J. M. Weber, J. Phys. Chem. A **114**, 8021 (2010).
[9]W. C. Lineberger and T. A. Patterson, Chem. Phys. Lett. **13**, 40 (1972).
[10]P. L. Jones, R. D. Mead, B. E. Kohler, S. D. Rosner, and W. C. Lineberger, J. Chem. Phys. **73**, 4419 (1980).
[11]K. K. Murray, K. R. Lykke, and W. C. Lineberger, Phys. Rev. A **36**, 699 (1987).
[12]T. Andersen, K. R. Lykke, D. M. Neumark, and W. C. Lineberger, J. Chem. Phys. **86**, 1858 (1987).
[13]E. A. Brinkman, E. Günther, O. Schafer, and J. I. Brauman, J. Chem. Phys. **100**, 1840 (1994).
[14]Y. X. Zhao, E. de Beer, C. S. Xu, T. Taylor, and D. M. Neumark, J. Chem. Phys. **105**, 4905 (1996).
[15]J. E. Mann, S. E. Waller, D. W. Rothgeb, and C. C. Jarrold, Chem. Phys. Lett. **506**, 31 (2011).
[16]H. T. Liu, D. L. Huang, Y. Liu, L. F. Cheung, P. D. Dau, C. G. Ning, and L. S. Wang, J. Phys. Chem. Lett. **6**, 637 (2015).
[17]A. S. Wightman, Phys. Rev. **77**, 521 (1950).
[18]R. F. Wallis, R. Herman, and H. W. Milnes, J. Mol. Spectrosc. **4**, 51 (1960).
[19]W. R. Garrett, Chem. Phys. Lett. **5**, 393 (1970).
[20]O. H. Crawford, Mol. Phys. **20**, 585 (1971).
[21]J. A. Stockdal, F. J. Davis, R. N. Compton, and C. E. Klots, J. Chem. Phys. **60**, 4279 (1974).
[22]H. Haberland, C. Ludewigt, H. G. Schindler, and D. R. Worsnop, J. Chem. Phys. **81**, 3742 (1984).
[23]C. Desfrancois, B. Baillon, J. P. Schermann, S. T. Arnold, J. H. Hendricks, and K. H. Bowen, Phys. Rev. Lett. **72**, 48 (1994).
[24]J. H. Hendricks, S. A. Lyapustina, H. L. de Clercq, J. T. Snodgrass, and K. H. Bowen, J. Chem. Phys. **104**, 7788 (1996).
[25]C. Desfrancois, V. Periquet, Y. Bouteiller, and J. P. Schermann, J. Phys. Chem. **102**, 1274 (1998).
[26]N. I. Hammer, K. Diri, K. D. Jordan, C. Desfrancois, and R. N. Compton, J. Chem. Phys. **119**, 3650 (2003).
[27]N. I. Hammer, R. J. Hinde, R. N. Compton, K. Diri, K. D. Jordan, D. Radisic, S. T. Stokes, and K. H. Bowen, J. Chem. Phys. **120**, 685 (2004).
[28]A. H. Zimmerman and J. I. Brauman, J. Chem. Phys. **66**, 5823 (1977).
[29]R. L. Jackson, A. H. Zimmerman, and J. I. Brauman, J. Chem. Phys. **71**, 2088 (1979).
[30]R. L. Jackson, P. C. Hiberty, and J. I. Brauman, J. Chem. Phys. **74**, 3705 (1981).
[31]D. A. Walthall, J. M. Karty, B. Ro1mer, O. Ursini, and J. I. Brauman, J. Phys. Chem. A **109**, 8785 (2005).
[32]K. R. Lykke, R. D. Mead, and W. C. Lineberger, Phys. Rev. Lett. **52**, 2221 (1984).
[33]R. D. Mead, K. R. Lykke, W. C. Lineberger, J. Marks, and J. I. Brauman, J. Chem. Phys. **81**, 4883 (1984).
[34]K. R. Lykke, D. M. Neumark, T. Andersen, V. J. Trapa, and W. C. Lineberger, J. Chem. Phys. **87**, 6842 (1987).

[35]J. Marks, J. I. Brauman, R. D. Mead, K. R. Lykke, and W. C. Lineberger, J. Chem. Phys. **88**, 6785 (1988).
[36]K. R. Lykke, K. K. Murray, D. M. Neumark, and W. C. Lineberger, Philos. Trans. R. Soc., A **324**, 179 (1988).
[37]D. M. Wetzel and J. I. Brauman, J. Chem. Phys. **90**, 68 (1989).
[38]K. Yokoyama, G. W. Leach, J. B. Kim, and W. C. Lineberger, J. Chem. Phys. **105**, 10696 (1996).
[39]K. Yokoyama, G. W. Leach, J. B. Kim, W. C. Lineberger, A. I. Boldyrev, and M. Gutowski, J. Chem. Phys. **105**, 10706 (1996).
[40]H. T. Liu, C. G. Ning, D. L. Huang, P. D. Dau, and L. S. Wang, Angew. Chem., Int. Ed. **52**, 8976 (2013).
[41]X. B. Wang and L. S. Wang, Rev. Sci. Instrum. **79**, 073108 (2008).
[42]P. D. Dau, H. T. Liu, D. L. Huang, and L. S. Wang, J. Chem. Phys. **137**, 116101 (2012).
[43]D. L. Huang, P. D. Dau, H. T. Liu, and L. S. Wang, J. Chem. Phys. **140**, 224315 (2014).
[44]R. S. Berry, J. Chem. Phys. **45**, 1228 (1966).
[45]J. Simons, J. Am. Chem. Soc. **103**, 3971 (1981).
[46]P. K. Acharya, R. A. Kendall, and J. Simons, J. Am. Chem. Soc. **106**, 3402 (1984).
[47]H. T. Liu, C. G. Ning, D. L. Huang, and L. S. Wang, Angew. Chem., Int. Ed. **53**, 2464 (2014).
[48]P. Chaudhuri and K. Wieghardt, Prog. Inorg. Chem. **50**, 151 (2001).
[49]S. Itoh, M. Taki, and S. Fukuzumi, Coord. Chem. Rev. **198**, 3 (2000).
[50]J. Platz, O. J. Nielsen, T. J. Wallington, J. C. Ball, M. D. Hurley, A. M. Straccia, W. F. Schneider, and J. Sehested, J. Phys. Chem. A **102**, 7964 (1998).
[51]C. W. Flickinger, Am. Ind. Hyg. Assoc. J. **37**, 596 (1976).
[52]S. G. Carmella, S. S. Hecht, T. C. Tso, and D. Hoffmann, J. Agric. Food Chem. **32**, 267 (1984).
[53]M. B. van Duursen, J. T. Sanderson, P. C. de Jong, M. Kraaij, and M. van den Berg, Toxicol. Sci. **81**, 316 (2004).
[54]A. M. Mebel and M. C. Lin, J. Am. Chem. Soc. **116**, 9577 (1994).
[55]I. Vedernikova, E. Proynov, D. Salahub, and A. Haemers, Int. J. Quantum Chem. **77**, 161 (2000).
[56]M. Nagaya, S. Kudoh, and M. Nakata, Chem. Phys. Lett. **432**, 446 (2006).
[57]M. Altarawneh, B. Z. Dlugogorski, E. M. Kennedy, and J. C. Mackie, J. Phys. Chem. A **114**, 1098 (2010).
[58]X. B. Wang, Q. A. Fu, and J. L. Yang, J. Phys. Chem. A **114**, 9083 (2010).
[59]I. Leon, Z. Yang, H. T. Liu, and L. S. Wang, Rev. Sci. Instrum. **85**, 083196 (2014).
[60]L. S. Wang, C. F. Ding, X. B. Wang, and S. E. Barlow, Rev. Sci. Instrum. **70**, 1957 (1999).
[61]H. T. Liu, Y. L. Wang, X. G. Xiong, P. D. Dau, Z. A. Piazza, D. L. Huang, C. Q. Xu, J. Li, and L. S. Wang, Chem. Sci. **3**, 3286 (2012).
[62]P. D. Dau, J. Su, H. T. Liu, D. L. Huang, J. Li, and L. S. Wang, J. Chem. Phys. **137**, 064315 (2012).
[63]G. A. Garcia, L. Nahon, and I. Powis, Rev. Sci. Instrum. **75**, 4989 (2004).
[64]V. Dribinski, A. Ossadtchi, V. A. Mandelshtam, and H. Reisler, Rev. Sci. Instrum. **73**, 2634 (2002).
[65]E. P. Wigner, Phys. Rev. **73**, 1002 (1948).
[66]U. Fano, Phys. Rev. **124**, 1866 (1961).
[67]S. T. Edwards, M. A. Johnson, and J. C. Tully, J. Chem. Phys. **136**, 154305 (2012).
[68]J. B. Kim, M. L. Weichman, T. I. Yacovitch, C. Shih, and D. M. Neumark, J. Chem. Phys. **139**, 104301 (2013).
[69]P. Hockett, M. Staniforth, and K. L. Reid, Phys. Rev. Lett. **102**, 253002 (2009).
[70]K. Regeta and M. Allan, Phys. Rev. Lett. **110**, 203201 (2013).